Carrier doping effect of humidity for single-crystal graphene on SiC

Makoto Kitaoka*, Takuya Nagahama, Kota Nakamura, Takuya Aritsuki, Kazuya Takashima, Yasuhide Ohno, and Masao Nagase

Tokushima University, Tokushima 770-8506, Japan

*E-mail: m_kitaoka@ee.tokushima-u.ac.jp

Carrier doping effects of water vapor and an adsorbed water layer on single-crystal graphene were evaluated. After annealing at 300 °C in nitrogen ambient, the sheet resistance of epitaxial graphene on a SiC substrate had a minimum value of 800 Ω/sq and the carrier density was estimated to be 1.2×10^{13} cm^{-2} for an n-type dopant. The adsorbed water layer, which acted as a p-type dopant with a carrier density of -7.4×10^{12} cm^{-2}, was formed by deionized (DI) water treatment. The sheet resistances of graphene samples increased with humidity, owing to the counter doping effect. The estimated p-type doping amounts of saturated water vapor were -2.5×10^{12} cm^{-2} for DI-water-treated graphene and -3.5×10^{12} cm^{-2} for annealed graphene.

1. Introduction

Graphene has attracted considerable attention for application in various electric devices owing to its superior electronic[1,2] and mechanical[3,4] properties. Since graphene is a two-dimensional material with a high ratio of surface area to volume, it is expected to be applied to high-sensitivity and selectivity sensors[5-8]. In addition, a graphene sensor is applicable to wearable sensors owing to its flexible nature[9]. In graphene sensors, gas molecules generally act as a carrier dopant for graphene. For example, NH_3 and CO molecules chemically induce electrons in graphene, whereas NO_2 and H_2O act as acceptors[5]. There are many reported results of sensitivity for various gas molecules[5-8,10-14]. For example, Melios et al. reported the humidity effect for CVD graphene on SiC[15]. However, these results were not quantitatively consistent with each other. Firstly, clean and high-quality single-crystal graphene will be required. The crosstalk effect between a target molecule and other environmental molecules must be fully understood for practical applications. In this context, investigating the effect of water molecules, which act as electron acceptors for graphene, is necessary for developing high-sensitivity graphene sensor devices. As previously reported, water molecules weakly adsorb on perfect free-standing graphene but graphene electronic transport properties are insensitive to perturbations by water adsorbates. Single molecules will not create any impurity states close to the Dirac point. On the other hand, it is well known that the effect of water adsorbates on graphene strongly depends on the properties of the substrate, such as the amount and type of defects[16]. In graphene transferred onto SiO_2, the dipole moments of H_2O adsorbates form local electrostatic fields that can shift the defect states of the substrate with respect to graphene electrons and result in doping[16]. The epitaxial graphene grown on a SiC substrate by thermal decomposition[17-23] is strongly electron doped (n-type) owing to the charge transfer between the SiC interface and graphene layers induced by SiC dangling bonds associated with interface defects[22-25]. In many reports, the effects of water adsorption on the graphene transferred onto SiO_2 substrates have been discussed[11,12,14,26]. However, there are few reports on the doping effect in the case of graphene on SiC substrates[6,10].

In this study, we investigated the characteristics of graphene–water interactions using high-quality single-crystal graphene on SiC substrates. We discussed the doping effect of the adsorbed water molecules and the structured water layer. We determined that the structured water layer formed by deionized (DI) water treatment very strongly interacted with graphene.

2. Experimental methods

2.1 Fabrication of graphene sample

Graphene samples were fabricated on 4H-SiC(0001) non-off-axis semi-insulating substrates. They were diced to 10 × 10 mm^2 by stealth dicing. Prior to high temperature annealing for graphene growth, the samples were cleaned using the following solutions: (1) DI water for 10 min, (2) sulfuric acid/hydrogen peroxide mixture for 5 min, (3) DI water rinse for 10 min, (4) dilute hydrofluoric acid for 1 min, and (5) DI water rinse for 15 min. After cleaning, the SiC substrate was subjected to high-temperature annealing for graphene growth at 1650 °C in an Ar environment (100 Torr) using a rapid thermal annealing system (SR1800, Thermo Riko). A single-crystal and high-quality graphene sample with a large area was fabricated[27,28]. The electrical properties of this large-area sample were measured by the van der Pauw method without any device fabrication processes, such as lithography with a resist and metallization. This method is preferable for preventing the effects of the resist residue and metal contamination[29-32]. The electrical mobility and carrier density before the experiments were measured by Hall effect measurement based on the van der Pauw method[28,33] with Au-coated contact pins on the four corners of graphene samples in air at room temperature. The magnetic field of a permanent NdFeB magnet for van der Pauw measurement is 261 mT.

2.2 Sample treatment

To investigate the characteristics of graphene–water interactions, we fabricated graphene by the thermal decomposition of SiC under three surface conditions, namely “untreated”, “DI-water-treated”, and “annealed”. In the untreated sample, no additional treatment after graphene growth was performed, except for storing in the atmosphere for few days. The DI-water-treated sample was obtained by immersion in DI water for 15 min. The annealed sample was prepared using a silica tube furnace at 300 °C in dry N_2.

2.3 Measurement system

A fabricated 10 × 10 mm^2 graphene sample was set on a spring clip board with four movable Au contacts and achieved contact with the electrode in an environmental control chamber, as shown in Fig. 1. The humidity in the chamber was controlled using a water bubbling system. Before starting the measurement, the chamber was purged with dry nitrogen for 15 h (54000 s) to remove the adsorbates from air. The humidity was controlled by ajusting the flow ratio of dry nitrogen to humid nitrogen at a total flow rate of 0.8 L/min. The duration of one period was 3 h (10800 s). The time dependence of the sheet resistance was measured in the four-terminal mode of Keithley 2430.

3. Results and discussion

3.1 Humidity control

Figure 2 shows the time dependence of relative humidity (RH). There were five periods and the flow rate of humid nitrogen was increased in the later periods (dry:humid = 4:0, 3:1, 2:2, 1:3, 0:4). Consequently, the humidity increased approximately 20%RH in one step.

3.2 Time dependence of sheet resistance

Time dependences of sheet resistances of untreated (red line), DI-water-treated (blue line), and annealed (green line) samples are shown in Fig. 3. The square plots indicate the end of each period. The sheet resistance increases with humidity in all the graphene samples. This result indicates that the carrier density of graphene decreases through the adsorption of water molecules. All graphene samples are electron doped, i.e., n-type doped, which was confirmed by Hall measurements before and after the experiments. Therefore, increasing the sheet resistance indicates a decrease in n-type carrier density, owing to counter doping with the p-type dopant adsorbed onto graphene. As shown in Fig. 2, the humidity did not completely saturate in each period owing to the large volume (approximately 13 L) of the environmental chamber. Half of the time constant was approximately 1200 s for each humidity step. The time constants of the sheet resistances shown in Fig. 3 are much larger than those of humidity. This result indicates that the water adsorption onto graphene on the SiC substrate has a very large time constant. This result is inconsistent with the results of previous studies of graphene humidity sensors[12,34]. In fact, this indicates that a complicated adsorption process occurs on the surface of graphene. In this work, it is difficult to estimate the adsorption rate of water molecules in graphene owing to a very low adsorption rate, i.e., the quantification of adsorption rate requires further investigation and is still open for discussion.

3.3 Humidity dependence of sheet resistance

Figure 4 shows the humidity dependence of sheet resistance at the end of each period derived from Figs. 2 and 3. The sheet resistance of graphene increased with humidity. The relationship between the sheet resistance and the humidity is almost linear for the DI-water-treated and annealed samples. On the other hand, the humidity dependence of the sheet resistance for the untreated sample was nonlinear. The sensitivity of the sheet resistance was very low at a low humidity (<40%RH). The sensitivity of the sheet resistance against humidity was derived from the slopes of the linear fits shown as solid lines in Fig. 4. The estimated sensitivities of the untreated, DI-water-treated, and annealed samples were 3.0×10^{-3}, 5.2×10^{-3}, and 1.9×10^{-3}%RH^{-1}, respectively. In this experiment, the DI-water-treated

sample was the most sensitive against humidity. As a result of eliminating the water effect, the lowest sheet resistance of 800 Ω was observed in the annealed sample in dry nitrogen. At a saturated humidity, the estimated sheet resistance of the annealed sample increased to approximately 900 Ω owing to the counter doping of water vapor molecules. On the other hand, the sheet resistance of the DI-water-treated sample was 1300 Ω in dry nitrogen, which is higher than that of the annealed sample at 100%RH. This result suggests that the p-type dopant layer was formed by DI water treatment. In the untreated sample, the additional p-dopant was adsorbed on the surface. The quantitative evaluation of the doping effect will be discussed in the following section.

3.4 Quantitative evaluation of doping effect of H_2O for graphene on SiC

The sheet resistance of two-dimensional materials is expressed as

$$R_S = \frac{1}{en_S\mu} \ , \qquad (1)$$

where $R_S, e, n_S,$ and μ are the sheet resistance, electron charge, sheet carrier density, and mobility, respectively. If the mobility does not change with sheet carrier density, the latter is directly calculated from the sheet resistance. As reported in the literature[27,35], the mobility of graphene strongly depends on the sheet carrier density and the relationship is expressed as

$$\mu = \alpha \frac{1}{\sqrt{n_S}} \ , \qquad (2)$$

where α is the proportionality constant. By using Eqs. (1) and (2), the sheet carrier density can be derived from the sheet resistance as follows:

$$n_S = \left(\frac{1}{e\alpha R_S}\right)^2 . \qquad (3)$$

Figure 5 shows the relationship between the carrier density and mobility of the samples before the humidity change experiments. The results for the DI-water-treated and annealed samples obey Eq. (2), where α is 2.4×10^9 $V^{-1}s^{-1}$, as shown in Fig. 5. However, the result for the untreated sample shows a different trend. This result suggests that unintentional impurities absorb on the surface of graphene stored in atmosphere for few days. The Hall measurement results of the DI-water-treated sample shown in Fig. 5 suggest that the DI water treatment can remove the unintentional impurities and initialize graphene surface conditions. In Fig. 5, the solid line shows the fitting curve of Eq. (2). The sheet resistance changes shown in Fig. 3 are converted to carrier density changes. Figure 6 shows the relationship between

the estimated sheet carrier density and the humidity. The doping amount of water vapor is estimated by subtracting the estimated carrier density in humid nitrogen from the corresponding value in dry nitrogen. The doping amount is maximum for a saturated water vapor pressure of 100%RH. The maximum doping amounts for the untreated, DI-water-treated, and annealed samples are -9.2×10^{11}, -2.5×10^{12}, and -3.5×10^{12} cm^{-2}, respectively. Since all the samples show negative values, the water molecules act as a p-type dopant. The doping amount of water vapor for the annealed sample is the largest among the three samples, whereas the sheet resistance sensitivity ($\Delta R/R_0$) of the annealed sample is the lowest, as shown in Table I. This result can be explained by the higher carrier density of the annealed sample. The estimated sheet carrier density at 0%RH for the annealed sample is 1.2×10^{13} cm^{-2} and those for the DI-water-treated and untreated samples are 4.2×10^{12} cm^{-2} and 2.2×10^{12} cm^{-2}, respectively. The carrier density of the annealed sample is approximately one order of magnitude higher than those of the other two samples. If the surface adsorbates on graphene were removed by annealing at 300 °C, the carrier density of the annealed sample would have an intrinsic value for graphene on SiC. This value, approximately 10^{13} cm^{-2}, is consistent with the carrier density estimated in ultra-high vacuum presented in the previous report[24]. Considering the carrier density of the annealed sample as a reference, the doping effect of DI water treatment is estimated to be (p-type) 7.4×10^{12} cm^{-2}. The doping amount of DI water treatment is much larger than that of water vapor. This result suggests that the DI water treatment forms other water adsorbate structures. From the discussed results, we believe that two adsorption mechanisms exist in the graphene–water interaction. One is the adsorption of water molecules of the order of 10^{12} cm^{-2}, which changes depending on humidity. The other is the formation of a structured water layer of the order of 10^{13} cm^{-2} by DI water treatment. To obtain the doping effect, highly ordered H_2O clusters or ice structures are required[16]. The doping of the structured water layer should be caused by H_2O clusters or ice structures formed on the graphene surface owing to the electrostatic fields induced by H_2O[16]. Our results clearly suggest that two water structures exist on graphene on the SiC substrate. A detailed investigation of water structures on graphene will be necessary. Now, we try to image the structured water layer by scanning probe microscopy. The results will be presented elsewhere. In the case of graphene on a 300-nm-thick oxide film (SiO_2), the relationship between the sheet carrier density and the gate voltage is given by $n_S = C_g V_g / e$[36], where the gate capacitance C_g is 115 aF μm^{-2}. The gate voltages converted from the sheet carrier densities for the adsorbed water molecules (3.5×10^{12} cm^{-2}) and structured water layer (7.4×10^{12} cm^{-2}) are 35 and 103 V, respectively. As a result of the conversion of

sheet carrier density to gate voltage, the Fermi level shift is large. The obtained high values indicate that the effect of water molecules cannot be ignored when a sensor device is fabricated using graphene on SiC. In particular, the doping ability of the structured water layer is high compared with those of the other reported chemical dopants (gas molecules and TCNQ) for graphene[5,37] and its effects on the electrical properties of graphene on SiC must be considered.

4. Conclusions

We elucidated the effect of water molecules adsorbed on epitaxial graphene. The sheet resistance changes of 10×10 mm^2-sized single-crystal graphene were evaluated by a simple four-terminal measurement method without the device fabrication process. Water molecules act as a very strong p-type dopant for graphene on a SiC substrate. The doping density of the structured water layer formed by DI water treatment was approximately 10^{13} cm^{-2}. Water molecules at 100%RH exhibited a hole-doping ability of approximately 3×10^{12} cm^{-2} for DI-water-treated and annealed samples. Since the humidity sensitivity of the sheet resistance depends on the initial carrier density of graphene, the sensitivity of the DI-water-treated sample was approximately three times higher than that of the annealed sample. Controlling the initial carrier density of graphene will be a key technique enabling the fabrication of the graphene sensor devices. DI water treatment will be an effective method for graphene surface cleaning. The results of the quantitative water-doping effect of epitaxial graphene will be useful for realizing graphene electronic devices.

Acknowledgments

This work was partially supported by JSPS KAKENHI Grant Numbers 26289107, 15H03551, 25110007, and 15H03986.

References

1) K. S. Novoselov, A. K. Geim, S. V. Morozov, D. Jiang, Y. Zhang, S. V. Dubonos, I. V. Grigorieva, and A. A. Firsov, Science **306**, 666 (2004).
2) K. I. Bolotin, K. J. Sikes, Z. Jiang, M. Klima, G. Fudenberg, J. Hone, P. Kim, and H. L. Stormer, Solid State Commun. **146**, 351 (2008).
3) K. S. Kim, Y. Zhao, H. Jang, S. Y. Lee, J. M. Kim, K. S. Kim, J. H. Ahn, P. Kim, J. Y. Choi, and B. H. Hong, Nature **457**, 706 (2009).
4) S. Bae, H. Kim, Y, Lee, X. Xu, J.-S. Park, Y. Zheng, J. Balakrishnan, T. Lei, H. R. Kim, Y. I. Song, Y.-J. Kim, K. S. Kim, B. Özyilmaz, J.-H. Ahn, B. H. Hong, and S. Iijima, Nat. Nanotechnol. **5**, 574 (2010).
5) F. Schedin, A. K. Geim, S. V. Morozov, E.W. Hill, P. Blake, M. I. Katsnelson, and K. S. Novoselov, Nat. Mater. **6**, 652 (2007).
6) V. K. Nagareddy, H. K. Chan, S. C. Hernández, V. D. Wheeler, R. L. Myers-Ward, L. O. Nyakiti, C. R. Eddy, Jr., S. G. Walton, J. P. Goss, N. G. Wright, D. K. Gaskill, and A. B. Horsfall, Appl. Phys. Lett. **102**, 173103 (2013).
7) S. Rumyantsev, G. Liu, M. S. Shur, R. A. Potyrailo, and A. A. Balandin, Nano Lett. **12**, 2294 (2012).
8) K. R. Amin and A. Bid, Appl. Phys. Lett. **106**, 183105 (2015).
9) J. J. Park, W. J. Hyun, S. C. Mun, Y. T. Park, and O. O. Park, ACS Appl. Mater. Interfaces **7**, 6317 (2015).
10) V. Panchal, C. E. Giusca, A. Lartsev, N. A. Martin, N. Cassidy, R. L. Myers-Ward, D. K. Gaskill, and O. Kazakova, 2D Mater. **3**, 015006 (2016).
11) C. Melios, A. Centeno, A. Zurutuza, V. Panchal, C. E. Giusca, S. Spencer, S. R. P. Silva, and O. Kazakova, Carbon **103**, 273 (2016).
12) M.-C. Chen, C.-L. Hsu, and T.-J. Hsueh, IEEE Electron Device Lett. **35**, 590 (2014).
13) E. R. Cortes, L. F. M. Solís, and J. S. Arellano, Rev. Mex. Fis. **59**, 118 (2013).
14) V. M. Bermudez and J. T. Robinson, Langmuir, **27**, 11026 (2011).
15) C. Melios, M. Winters, W. Strupiński, V. Panchal, C. E. Giusca, K. D. G. Imalka Jayawardena, N. Rorsman, S. Ravi, P. Silva, and O. Kazakova, Nanoscale **9**, 3440 (2017).
16) T. O. Wehling, A. I. Lichtenstein, and M. I. Katsnelson, Appl. Phys. Lett. **93**, 202110 (2008).
17) J. Borysiuk, R. Bożek, W. Strupiński, A. Wysmołek, K. Grodecki, R. Stępniewski, and J. M. Baranowski, J. Appl. Phys. **105**, 023503 (2009).
18) A. Fissel, Phys. Rep. **379**, 149 (2003).

19) C. Berger, Z. Song, T. Li, X. Li, A. Y. Ogbazghi, R. Feng, Z. Dai, A. N. Marchenkov, E. H. Conrad, P. N. First, and W. A. de Heer, J. Phys. Chem. B **108**, 19912 (2004).
20) K. V. Emtsev, A. Bostwick, K. Horn, J. Jobst, G. L. Kellogg, L. Ley, J. L. McChesney, T. Ohta, S. A. Reshanov, J. Röhrl, E. Rotenberg, A. K. Schmid, D. Waldmann, H. B. Weber, and T. Seyller, Nat. Mater. **8**, 203 (2009).
21) M. Kusunoki, W. Norimatsu, J. Bao, K. Morita, and U. Starke, J. Phys. Soc. Jpn. **84**, 121014 (2015).
22) F. Varchon, R. Feng, J. Hass, X. Li, B. N. Nguyen, C. Naud, P. Malled, J.-Y. Veuillen, C. Berger, E. H. Conrad, and L. Magaud, Phys. Rev. Lett. **99**, 12685 (2007).
23) J. Hass, W. A. De Heer, and E. H. Conrad. J. Phys.: Condens. Matter **20**, 323202 (2008).
24) T. Ohta, A. Bostwick, T. Seyller, K. Horn, and E. Rotenberg, Science **313**, 951 (2006).
25) S. Kopylov, A. Tzalenchuk, S. Kubatkin, and V. I. Fal'ko, Appl. Phys. Lett. **97**, 112109 (2010).
26) M. J. Lee, J. S. Choi, J.-S. Kim, I.-S. Byun, D. H. Lee, S. Ryu, C. Lee, and B. H. Park, Nano Res. **5**, 710 (2012).
27) T. Aritsuki, T. Nakashima, K. Kobayashi, Y. Ohno, and M. Nagase, Jpn. J. Appl. Phys. **55**, 06GF03 (2016).
28) K. Kobayashi, S. Tanabe, T. Tao, T. Okumura, T. Nakashima, T. Aritsuki, R.-S. O, and M. Nagase, Appl. Phys. Express **8**, 036602 (2015).
29) A. Pirkle, J. Chan, A. Venugopal, D. Hinojos, C. W. Magnuson, S. McDonnell, L. Colombo, E. M. Vogel, R. S. Ruoff, and R. M. Wallace, Appl. Phys. Lett. **99**, 122108 (2011).
30) M. Kratzer, B. C. Bayer, P. R. Kidambi, A. Matković, R. Gajić, A. Cabrero-Vilatela, R. S. Weatherup, S. Hofmann, and C. Teichert, Appl. Phys. Lett. **106**, 103101 (2015).
31) S. Kim, S. Shin, T. Kim, H. Du, M. Sung, C. Lee, K. Kim, S. Cho, D. H. Seo, and S. Seo, Carbon **98**, 352 (2016).
32) Z. Cheng, Q. Zhou, C. Wang, Q. Li, C. Wang, and Y. Fang, Nano Lett. **11**, 767 (2011).
33) L. J. van der Pauw, Philips Res. Rep. **13** 1 (1958).
34) A. Ghosh, D. J. Late, L. S. Panchakarla, A. Govindaraj, and C. N. R. Rao, J. Exp. Nanosci. **4**, 313 (2009).
35) Y.-W. Tan, Y. Zhang, K. Bolotin, Y. Zhao, S. Adam, E. H. Hwang, S. Das Sarma, H. L. Stormer, and P. Kim, Phys. Rev. Lett. **99**, 246803 (2007).
36) Y. Zhang, Y.-W. Tan, H. L. Stormer, and P. Kim, Nature **438**, 201 (2005).
37) C. Coletti, C. Riedl, D. S. Lee, B. Kraus, L. Patthey, K. von Klitzing, J. H. Smet, and U.

Starke, Phys. Rev. B **81,** 235401 (2010).

Figure Captions

Fig. 1. (Color online) Measurement system for humidity control using bubbling system and Hall effect based on van der Pauw method, with spring clip board with four Au contact pins.

Fig. 2. (Color online) Humidity control procedure. The flow rate was changed every 3 h (10800 s).

Fig. 3. (Color online) Time dependences of sheet resistances of untreated (red line), DI-water-treated (blue line), and annealed (green line) samples. The plots show the humidity saturation points.

Fig. 4. (Color online) Dependence of sheet resistance on humidity for each sample, derived from Figs. 2 and 3. The plots indicate the values at the end of the period of humidity change. The solid lines show the linear fitting of the data.

Fig. 5. (Color online) Relationship between mobility and sheet carrier density measured by Hall effect based on van der Pauw method, for untreated (red circle), DI-water-treated (blue square), and annealed (green triangle) samples. The fitted line is drawn using the data of DI-water-treated and annealed samples.

Fig. 6. (Color) Dependence of sheet carrier density on humidity.

Table I. Summary of the sensitivity based on resistance, estimated doping amount at 100%RH, and estimated carrier density at 0%RH for each sample.

Sample	$\Delta R/R_0$ (%RH^{-1})	Estimated doping amount at 100%RH (cm^{-2})	Estimated carrier density at 0%RH (cm^{-2})
Untreated	3.0×10^{-3}	9.2×10^{11}	2.2×10^{12}
DI-water-treated	5.2×10^{-3}	2.5×10^{12}	4.2×10^{12}
Annealed	1.9×10^{-3}	3.5×10^{12}	1.2×10^{13}

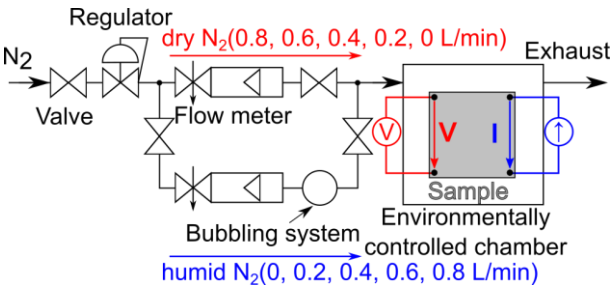

Fig.1. (Color Online)

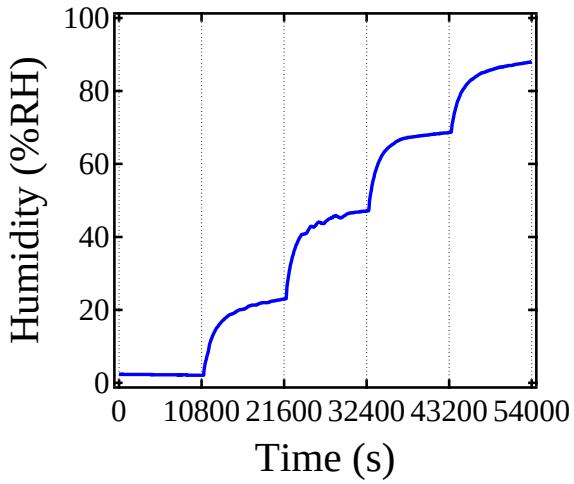

Fig.2. (Color Online)

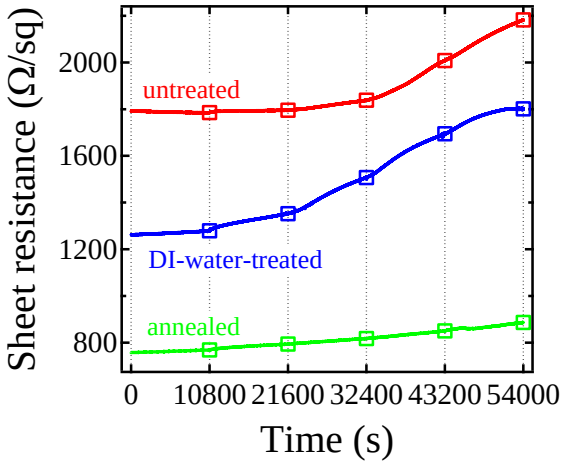

Fig.3. (Color Online)

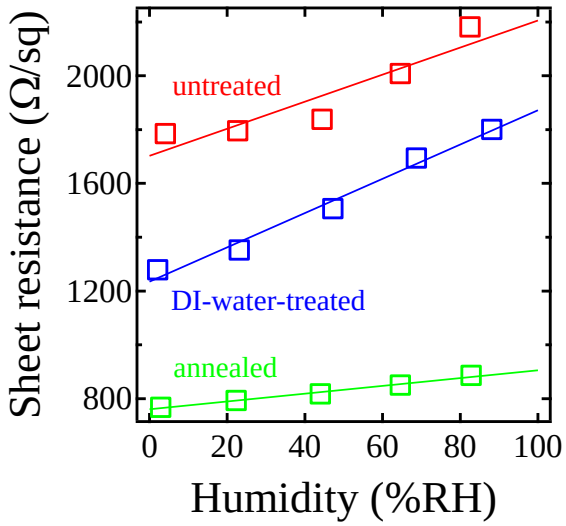

Fig.4. (Color Online)

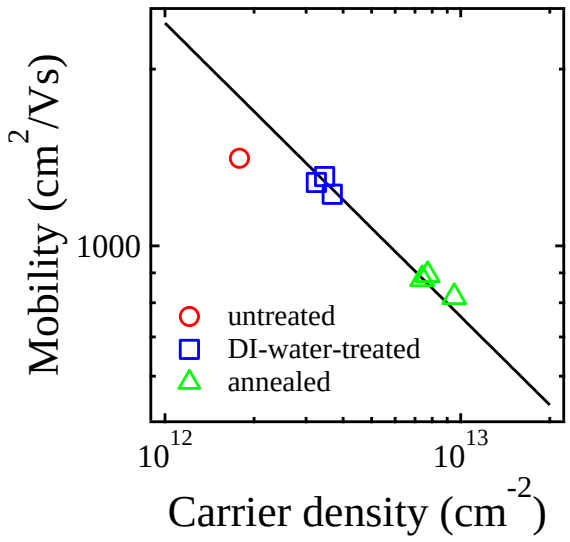

Fig.5. (Color Online)

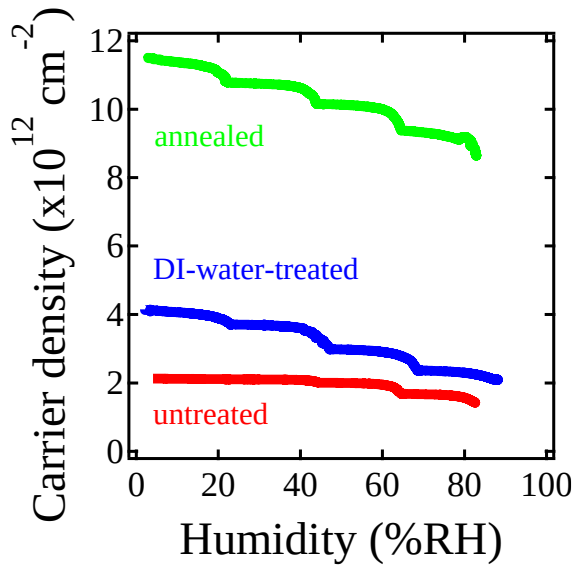

Fig.6. (Color Online)